electronics

MDPI

Article

An Adjustable Parameter-Based Robust Distributed Fault Diagnosis for One-Sided Lipschitz Formation of Clustered Multi-Agent Systems

Ailin Barzegar and Afshin Rahimi *

Department of Mechanical, Automotive and Materials Engineering, University of Windsor, Windsor, ON N9B 3P4, Canada; barzegaa@uwindsor.ca
* Correspondence: arahimi@uwindsor.ca

Abstract: This paper addresses the challenge of distributed fault diagnosis in the context of the one-sided Lipschitz formation of agents. Each agent integrates an observer to detect and estimate both linear and non-linear faults in its attitude control subsystem. A robust design configuration is also developed to account for external perturbations. The robust observer utilized in this study is an unknown input observer (UIO), designed to mitigate the impact of disturbances on fault and state estimation errors. The observer's parameters are determined using linear matrix inequalities (LMIs). Furthermore, a UIO incorporating an adjustable parameter (AP) is introduced to enhance fault diagnosis accuracy. Simulation results for two satellite clusters, consisting of five satellites with varying dynamics due to external disturbances, are presented to validate the approach. Instead of equipping every agent with an observer, specific agents can be equipped with observers to detect faults throughout the constellation, thereby reducing computational demands in configurations with numerous agents. Finally, a comparison is made between the proposed AP-based UIO and a standard UIO. The comparison findings reveal a noteworthy average of a substantial 56.61% reduction in root mean square error (RMSE) employing AP-based UIO compared to the utilization of standard robust UIO.

Keywords: distributed fault diagnosis; adjustable parameter; unknown input observer; formation control; clustered multi-agent systems

check for updates

Citation: Barzegar, A.; Rahimi, A. An Adjustable Parameter-Based Robust Distributed Fault Diagnosis for One-Sided Lipschitz Formation of Clustered Multi-Agent Systems. *Electronics* **2024**, *13*, 2759. https://doi.org/10.3390/electronics13142759

Academic Editors: Parivallal Arumugam, Ramasamy Kavikumar, S. A. Karthick and Saša Mladenović

Received: 30 May 2024
Revised: 1 July 2024
Accepted: 11 July 2024
Published: 13 July 2024

Copyright: © 2024 by the authors. Licensee MDPI, Basel, Switzerland. This article is an open access article distributed under the terms and conditions of the Creative Commons Attribution (CC BY) license (https://creativecommons.org/licenses/by/4.0/).

1. Introduction

Multi-agent systems (MASs) comprise multiple agents, and they offer a strategy by which to decompose complex systems into more manageable and simplified components. The control of MASs centers around four primary categories: consensus, formation, flocking, and coverage management [1].

One of the core objectives of formation control is to ensure that agents conform to a predefined arrangement. Effective formation control strategies can benefit various collaborative endeavors, such as coordinating agent clusters. This approach can enhance mission resilience, image quality, and stability [2]. The real-world scenarios might necessitate instances where agents must be integrated into clusters. It is important to note that the agents within each cluster could exhibit diverse geometric configurations and dynamics [3].

In recent decades, the exploration of MASs has been extensively studied across various domains and applications, from engineering to finance [4–7]. Because of demanding operational scenarios, this increase highlights the requirement for improved reliability. MASs exhibit the limitation of high vulnerability to faults and inaccuracies in contrast to an integrated system. Additionally, the malfunction of a single unit can be transmitted through topological associations to its connected nodes, impacting the overall system's efficiency. In light of this, system safety becomes a top priority.

Scientific research is increasingly interested in fault diagnosis, a systematic methodology that entails the precise detection, isolation, and identification of underlying faults [8–10]. A fault detection and isolation (FDI) system serves the purpose of identifying and localizing faults, ensuring its capability to detect the existence of faults and precisely pinpoint their specific locations. The final step of fault diagnosis, i.e., fault identification, holds paramount significance. It is vital in yielding comprehensive insights into the fault's geometric attributes and dimensions. This pivotal phase plays a crucial role in enhancing our understanding of fault characteristics, thus contributing substantially to the overall accuracy and depth of fault analysis [11]. The data derived from the fault diagnosis process will be utilized for fault-tolerant control (FTC). FTC methods can generally be divided into active and passive approaches. A substantial amount of literature focuses on passive FTC or robust methods, as shown by references [12–15]. However, in certain cases, the nature of faults can threaten the controller's stability and performance, posing a challenge that robust control theories or passive FTC cannot effectively address. Active FTC encompasses two primary strategies: (i) fault accommodation and (ii) reconfiguration. Minor faults can be effectively managed through fault accommodation, which involves adjusting the controller parameters to match those of the faulty plant. This process requires modifying the control algorithm when a fault is detected while maintaining the system components active and operational. The plant's input and output, vital elements in the control loop, remain consistent with the fault-free scenario [12]. Conversely, when applying various fault reconfiguration strategies, the control loop is restructured to align the controller with the affected plant. To monitor faults in MASs, current FTC approaches can be categorized into four main groups: (i) individual methodologies; (ii) cooperative methodologies; (iii) topology reconfiguration-based methodologies; and (iv) composition reconfiguration-based methodologies [16].

As for fault diagnosis techniques, several widely used methods exist, including the model-based approach, data-driven methodologies, expert systems, and hybrid strategies [2]. In the present context, our study undertakes a comprehensive exploration of the model-based fault diagnosis techniques, considering their significance within the larger landscape of fault detection and mitigation.

In recent decades, there has been an emphasis on research initiatives concerning the fault diagnosis process within agent formation flying (SFF). An innovative fault detection (FD) system rooted in a decentralized dynamic neural network (DNN) framework was designed specifically for monitoring the reaction wheels of agents engaged in a formation flying mission in [17]. A distributed method for identifying, locating, and calculating actuator failures across SFF is studied in [18]. The primary goal in [19] is to design a DNN-based strategy for FDI in pulsed plasma thrusters. These thrusters are integral to the attitude control subsystem of satellites assigned to perform formation flying missions. The central emphasis lies in advancing the dependability and efficiency of pulsed plasma thrusters, contributing significantly to the successful accomplishment of formation flying missions [19]. Azizi and Khorasani [20] introduced a distributed Kalman filter approach designed to estimate actuator faults in satellites engaged in deep space formation flying. This method's applicability extends beyond space missions, encircling expansive domains like sensor networks and power systems.

Further to their earlier work, Azizi and Khorasani [21] introduced an innovative hybrid-switching framework designed to cater to the intricate task of cooperative actuator fault estimation among SFFs operating in deep space. They aim to significantly enhance the precision and robustness of the fault estimation process within the distinct operational parameters of deep space missions. Ghasemi and Khorasani [22] presented a pioneering FDI strategy customized for the attitude control system of SFF. This novel approach employs the power of extended Kalman filters (EKFs) [22]. These filters are used mainly within three distinctive architectural frameworks: decentralized, centralized, and semi-decentralized. Meskin and Khorasani [23] implemented a novel FDI technique for SFF using the multiple-input, multiple-output (MIMO) formation control architecture. Han et al. [24] explored

a resilient H_∞ distributed fault estimation observer (DFEO) methodology applied to synchronizing attitudes across multiple satellites. Within this framework, they constructed robust H_∞ DFEO modules at each satellite to effectively estimate intermittent faults during the mission.

Barzegar and Rahimi [25] investigated the challenge of distributed fault identification and assessment within the formation of satellite clusters. An observer was integrated into each satellite, capable of fault detection and assessing their scale and dynamics over time. Additionally, this exploration involved formulating a formation plan, even in the presence of external disturbances and faults.

External disturbances have a notable impact on fault diagnosis accuracy in multi-satellite systems. Employing optimization computations to enhance residual responsiveness to faults while increasing resilience against disturbances is an effective approach. Unknown input observer (UIO)-based methods are valuable for isolating disturbances as an unknown input from the fault estimation procedure. Gao et al. [26] developed a UIO to mitigate the effects of disturbances on sensor faults. Moreover, in addition to the utilization of the UIO, the employment of the H_∞ approach serves to fortify the robustness of the observer.

In many MAS fault diagnosis methods, agents can estimate faults in themselves or nearby agents [27,28]. However, practical situations may require observers for specific agents instead of all to reduce costs and computational load. To minimize expenses and computational demands, observers should focus on estimating states and faults in individual agents and their neighbors. Addressing this, Rahimi and Ahmadpour [29] explored a distributed UIO-based approach, aiming to approximate the faults of each agent and its neighbors.

The enhancement in fault estimation performance can be achieved by incorporating adjustable parameters (APs) into the observer's design. Introducing these APs grants the distributed fault diagnosis increased flexibility in its design process and quantitatively enhances its fault estimation capabilities. A novel approach involving an AP-based DFEO addresses this advancement [28,30]. This innovation is tailored for MASs characterized by directed communication topologies and encompasses linear system models, as studied in [28], and non-linear system models, as discussed in [30].

Motivated by the reviewed literature, the current study contributions are as follows:

1. A fault diagnosis approach for two distinct clusters of agents, each operating under unique environmental conditions with varying external disturbances. Previous studies have explored FDI in MASs with diverse dynamics [31–33], and the FTC problem within the cluster consensus framework has been addressed in [34]. It is worth noting that few existing approaches in the literature address fault detection and estimation for agents belonging to separate clusters and exposed to dissimilar environmental conditions. The primary focus is developing a method using UIOs for distributed fault detection and estimation within satellite cluster formations.
2. Integrating APs into the observer's design enhances fault estimation performance and contributes to this overall improvement. Compared with the work in [25], referred to as *simple UIO* in this study, this study focuses on developing AP-based distributed fault diagnosis. It represents the first investigation of using AP and UIO for time-varying fault diagnosis across the formation of satellites belonging to different clusters. Compared to the AP-based observer design in [28,30], the present study exhibits advancements on several fronts. First, it introduces a novel UIO mechanism to decouple the influence of disturbances from fault estimation errors effectively. Second, it explores a broader spectrum of non-linear functions, enhancing the model's adaptability. Third, the study delves into incorporating weighted clusters of agents, expanding the scope of analysis and applicability.
3. The MAS demonstrates one-sided Lipschitz non-linearity, offering a comprehensive framework for modeling various practical non-linear systems [35]. In recent years, the utilization of one-sided non-linear systems for fault diagnosis and consensus control

in MASs has garnered significant interest [36–39]. Compared to existing literature, this study marks the pioneering exploration of one-sided non-linearities for the distributed robust fault diagnosis of clustered MASs.

The rest of this paper is organized as follows: The foundational concepts, system descriptions, and strategies for cluster formation control and AP-based robust fault diagnosis observer design are discussed in Section 2. The outcomes of simulations are presented in Section 3, and future research directions are outlined in Section 4. Finally, Section 5 summarizes the concluding remarks.

2. Methodology

This section details the communication topology and agent dynamics, providing a foundation for the subsequent discussion on the control approach and fault diagnosis in the proposed methodology.

2.1. Graph Preliminaries

The interactions between agents are commonly shown in interaction graphs. This section presents essential conventions in graph representation:

A graph primarily consists of nodes denoted as $\vartheta = \{\vartheta_1, \vartheta_2, \ldots, \vartheta_N\}$ alongside edges indicated by $\varepsilon \subseteq \vartheta \times \vartheta$. The weight of each connection is portrayed within the components of the adjacency matrix, $A = [a_{nj}] \in R^{N \times N}$. Specifically, $a_{nj} = 1$, when a communication path exists from node n to node j; otherwise, $a_{nj} = 0$. Directed edges form connections between groups of nodes, creating directed graphs. Conversely, undirected graphs adhere to the relationship $a_{nj} = a_{jn}$.

Regarding notations, a given matrix N is identified as both positive definite ($N > 0$) and positive semidefinite ($N \geq 0$). Matrix I represents the identity matrix with appropriate dimensions. The Kronecker product of matrices K and J is denoted as $K \bigotimes J$, is an operation on two matrices of arbitrary size resulting in a block matrix. Given two matrices K of size $m \times n$ and J of size $p \times q$, the Kronecker product $K \bigotimes J$ is defined as an $mp \times nq$ matrix formed by multiplying each element of K by the entire matrix J.

2.2. System Architecture

The behavior exhibited by agent r within MASs can be described using the following dynamics:

$$\dot{x}_r(t) = A_{1x}x_r(t) + A_{1u}u_r(t) + A_{1w}w_r(x_r(t)) + A_{1f}f_r(t) + A_{1d}d_r(t), \tag{1}$$

$$y_r(t) = C_1 x_r(t), \tag{2}$$

where the system states are denoted as $x_r(t) \in R^{n_x}$, and the control input for agent r is expressed as $u_r(t) \in R^{n_u}$. Furthermore, the potential fault within the system is $f_r(t) \in R^{n_f}$, while the disturbance element is $d_r(t) \in R^{n_d}$. Additionally, the output vector of the rth agent is represented as $y_r(t) \in R^{n_y}$. Matrices $A_{1x}, A_{1u}, A_{1w}, A_{1f}, A_{1d}$, and C_1 are all of compatible dimensions.

The information regarding the one-sided Lipschitz non-linear function $w_r(x_r(t)) \in R^{n_w}$, in relation to $x_r(t)$ is available and the condition is presented in (3) [40]. In the context of this research, we denote the one-sided Lipschitz constant as "L" to quantify specific properties. The constant L can differ depending on various working conditions, such as working in separate clusters of agents.

$$\langle w_r(x_{r1}(t)) - w_r(x_{r2}(t)), x_{r1}(t) - x_{r2}(t) \rangle \leq L_i \parallel x_{r1}(t) - x_{r2}(t) \parallel^2 \tag{3}$$

Remark 1. *The one-sided Lipschitz non-linearities encompass many practical non-linear systems, including classic Lipschitz conditions as specific cases. Research indicates that one-sided Lipschitz constants are smaller than classical Lipschitz constants. This reduction lessens conservatism when addressing linear matrix inequalities (LMIs) involving Lipschitz non-linearities, such as*

in [25]. Notably, one-sided Lipschitz constants can assume zero or negative values, unlike Lipschitz constants, which must remain positive. Any Lipschitz function also qualifies as a one-sided Lipschitz function. However, the converse is not necessarily true [36].

Lemma 1. ([41]). *For a given matrix P, we have the following:*

- *The set $\mathcal{D}(O, r)$ representing a closed circular region with a center at O and a radius of r.*
- *The eigenvalues of matrix P are situated within the confines of the circular region.*

Then, it can be assumed that a positive definite symmetric matrix $Y = Y^T > 0$ exists, which fulfills the given conditions.

$$\begin{bmatrix} -Y & YP - OY \\ * & -r^2 Y \end{bmatrix} < 0$$

Lemma 2. ([42]). *Assume that matrices Z_1 and Z_2 possess suitable dimensions, and there exists a positive constant ρ such that*

$$Z_1 Z_2^T + Z_2 Z_1^T \leq (1/\rho) Z_1 Z_1^T + \rho Z_2 Z_2^T.$$

This concludes the required foundations to discuss the proposed methodology in the next section.

2.3. Proposed Methodology

This section explores the topic of formation control concerning one-sided Lipschitz non-linear MASs. Furthermore, a UIO is detailed to detect and estimate faults to mitigate disturbances and achieve partial decoupling.

In [23], a classification of five primary SFF control architectures is introduced: (i) MIMO; (ii) leader–follower; (iii) virtual structure; (iv) cyclic; and (v) behavioral. Leader–follower and virtual structure approaches stand out as the prevailing strategies in SFF control. Within the leader–follower approach, a designated leader satellite dictates the desired motion for the other satellites in the formation. In contrast, the virtual structure method imparts the desired motion to a satellite by implementing an abstract geometric framework. This framework can vary for every cluster.

Given the description of MASs outlined in (1) and (2), an algorithm for forming clusters within the MAS framework comprising R agents is provided as follows [43]:

$$u_r(t) = mK\left(\sum_{i \in R} a_{ri}[X_i(t) - X_r(t) - d_{ri}]\right), \tag{4}$$

where $m > 0$ is coupling gain, K represents the feedback gain matrix, and d_{ri} is a predetermined and constant distance between agents within the system.

To detect and estimate faults within MASs, if we consider an augmented state that encompasses both the states and faults of individual agents, denoted as $\bar{x}_r(t) = \left[x_r^T(t), f_r^T(t)\right]^T$, then it is possible to transform the equations of the MASs (1) and (2) as follows:

$$\dot{\bar{x}}_r(t) = A_{2x}\bar{x}_r(t) + A_{2u}u_r(t) + A_{2w}w_r(x_r(t)) + A_{2f}f_r(t) + A_{2d}d_r(t), \tag{5}$$

$$y_r(t) = C_2\bar{x}_r(t), \tag{6}$$

employing the given matrices,

$$\begin{gathered} A_{2x} = \begin{bmatrix} A_1 & A_{1f} \\ 0 & 0 \end{bmatrix}, A_{2u} = \begin{bmatrix} A_{1u} \\ 0 \end{bmatrix}, \\ A_{2d} = \begin{bmatrix} A_{1d} \\ 0 \end{bmatrix}, A_{2w} = \begin{bmatrix} A_{1w} \\ 0 \end{bmatrix}, C_2 = \begin{bmatrix} C_1 & 0 \end{bmatrix}, A_{2f} = \begin{bmatrix} 0 \\ A_{1f} \end{bmatrix}. \end{gathered} \tag{7}$$

A UIO can be employed to identify and approximate faults present in both the agent and its neighbors.

By merging the state vectors of a specific agent and all of its neighboring agents, the collective state vector for the entire MASs is constructed.

$$X_{(r)}(t) = \begin{bmatrix} x_{r1}(t) \\ x_{r2}(t) \\ \vdots \\ x_{rR}(t) \end{bmatrix} \tag{8}$$

Let us merge the augmented form of the state vector of one agent and its neighbor and build a global augmented state vector,

$$\overline{X}_{(r)}(t) = \begin{bmatrix} \overline{X}_{r1}(t) \\ \overline{X}_{r2}(t) \\ \vdots \\ \overline{X}_{rR}(t) \end{bmatrix}, \tag{9}$$

where $\bar{X}_{ri}(t) = \left[x_{ri}^T(t), f_{ri}^T(t)\right]^T, i \in \{1, \ldots, R\}$. Hence, the agents' dynamics can be summarized as follows:

$$\dot{\overline{X}}_r(t) = A_{3x}\overline{X}_r(t) + A_{3u}U_r(t) + A_{3w}W(x_r(t)) + A_{3f}\overline{F}_r(t) + A_{3d}\overline{D}_r(t), \tag{10}$$

$$Y_r(t) = C_3\overline{x}_r(t), \tag{11}$$

$$\begin{gathered} A_{3x} = I_R \otimes A_2, B_{3u} = I_R \otimes B_{2u}, \\ B_{3d} = I_R \otimes B_{2d}, B_{3w} = I_R \otimes B_{2w}, \\ C_3 = I_R \otimes C_2, B_{3f} = I_R \otimes B_{2f}, \end{gathered} \tag{12}$$

where

$$W\left(x_{(r)}(t)\right) = \begin{bmatrix} w_{r1}(x_{r1}(t)) \\ w_{r2}(x_{r2}(t)) \\ \vdots \\ w_{rR}(x_{rR}(t)) \end{bmatrix}, \overline{F}_{(r)}(t) = \begin{bmatrix} \bar{f}_{r1}(t) \\ \bar{f}_{r2}(t) \\ \vdots \\ \bar{f}_{rR}(t) \end{bmatrix}, \overline{D}_{(r)}(t) = \begin{bmatrix} d_{r1}(t) \\ d_{r2}(t) \\ \vdots \\ d_{rN}(t) \end{bmatrix}, U_{(r)}(t) = \begin{bmatrix} u_{r1}(t) \\ u_{r2}(t) \\ \vdots \\ u_{rR}(t) \end{bmatrix}, Y_{(r)}(t) = \begin{bmatrix} y_{r1}(t) \\ y_{r2}(t) \\ \vdots \\ y_{rR}(t) \end{bmatrix}. \tag{13}$$

The UIO associated with the system derived in (10) and (11) equipped with APs ($H_{(r)}$ and $R_{1(r)}$) to improve fault diagnosis precision can be formed as follows:

$$\begin{gathered} \dot{\Omega}_{(\mathrm{r})}(t) = T_{(r)}\Omega_{(\mathrm{r})}(t) + \mathbb{C}_{(r)}U_{(\mathrm{r})}(t) + \left(I - \theta_{(r)}C_2\right)A_{2\mathrm{w}}W\left(\hat{\mathcal{X}}_{(r)}(t)\right) \\ +\lambda_{(r)}Y_{(r)}(t) + G_{(r)1(r)}\left(Y_{(r)}(t) - \hat{Y}_{(r)}(t)\right) + H_{(r)}R_{1(r)1(r)}\left(\dot{Y}_{(r)}(t) - \hat{\dot{Y}}_{(r)}(t)\right), \end{gathered} \tag{14}$$

$$\hat{\overline{\mathcal{X}}}_{(r)}(t) = \Omega_{(r)}(t) + \theta_{(r)}Y_{(r)}(t), \tag{15}$$

where

$$\mu_{1(r)} = diag\{a_{1r}, a_{2r}, \ldots, a_{Rr}\} \otimes I_{n_y}, \tag{16}$$

$$\hat{Y}_{(r)}(t) = C_{3(r)}\hat{\bar{X}}_{(r)}(t). \tag{17}$$

Initially, it is essential to outline the necessary assumption that must be satisfied for the viability of the proposed UIO. Subsequently, the error dynamics can be formed and discussed.

Assumption 1. *The AP-based UIO here aims to isolate a portion of disturbances, thereby mitigating the adverse effects caused by the remaining disturbance components. The system must satisfy the following requirements to design the UIO (15) according to the abovementioned conditions.*

$$rank([C_2 A_{d1}]) = rank([A_{d1}]) = rank([(I_R \otimes C_1)(I_R \otimes A_{d1})]) = rank\ ([(I_R \otimes A_{d1})]) \quad (18)$$

This implies that vector $d_r(t)$ can be formulated as $d_r(t) = \left[d_{r,1}^T(t)\ d_{r,2}^T(t)\right]^T$. It is assumed that $d_{r,1}(t)$ can undergo decoupling, unlike $d_{r,2}(t)$. Furthermore, a condition is placed such that the matrix $A_{1d} = \begin{bmatrix} A_{d1} & A_{d2} \end{bmatrix}$, where the matrix A_{d1} possesses a full-column rank.

States and output residuals can be ascertained using the following procedure:

$$\begin{aligned} \widetilde{\mathcal{X}}_{(r)}(t) &= \overline{\mathcal{X}}_{(r)}(t) - \hat{\overline{\mathcal{X}}}_{(r)}(t) \\ \widetilde{Y}_{(r)}(t) &= Y_{(r)}(t) - \hat{Y}_{(r)}(t). \end{aligned} \quad (19)$$

Consequently, the error dynamics can be described as follows:

$$\begin{aligned} \epsilon_{(r)}(t) &= \overline{\mathcal{X}}(t) - \hat{\overline{\mathcal{X}}}(t) = \overline{\mathcal{X}}_{(\mathrm{r})}(t) - \Omega_{(\mathrm{r})}(t) - \theta_{(r)} Y_{(\mathrm{r})}(t)\Big) \\ &= \Big(I - \theta_{(r)} C_{2(r)}\Big)\overline{\mathcal{X}}_{(\mathrm{r})}(t) - \Omega_{(\mathrm{r})}(t) = \Big(\alpha_{(r)}\Big)\overline{\mathcal{X}}_{(r)}(t) - \Omega_{(r)}(t). \end{aligned} \quad (20)$$

We adopt the assumption that $\alpha_{(r)} = I - \beta_{(r)} C_{2(r)}$. Regarding the derivative of the error, we have the following:

$$\begin{aligned} \dot{\epsilon}_{(r)}(t) = \Big(\alpha_{(r)}\Big)\dot{\overline{\mathcal{X}}}_{(r)}(t) - \dot{\Omega}_{(r)}(t) = \alpha_{(r)}\Big(A_{2\mathrm{x}}\overline{\mathcal{X}}_{(\mathrm{r})}(t) + A_{2\mathrm{u}}U_{(\mathrm{r})}(t) + A_{2\mathrm{w}}W\Big(\mathcal{X}_{(r)}(t)\Big)\Big) \\ + A_{\mathrm{d1}}\overline{D}_{(r),1}(t) + A_{\mathrm{d2}}\overline{D}_{(r),2}(t)) - \Big(T_{(r)}\Omega_{(\mathrm{r})}(t) + \complement_{(r)}U_{(\mathrm{r})}(t) + \Big(I - \theta_{(r)}C_{2(r)}\Big)A_{2\mathrm{w}}G\Big(\hat{\overline{\mathcal{X}}}_{(\mathrm{r})}(t)\Big) \\ + \lambda_{(r)}y_{(r)}(t) + G_{(r)1(r)}\Big(Y_{(r)}(t) - \hat{Y}_{(r)}(t)\Big) + H_{(r)}R_{1(r)1(r)}\Big(\dot{Y}_{(r)}(t) - \hat{\dot{Y}}_{(r)}(t)\Big)\Big). \end{aligned} \quad (21)$$

The following is a derivation of error by applying (15):

$$\begin{aligned} \dot{\epsilon}_{(r)}(t) = \alpha_{(r)}A_{2x}\overline{\mathcal{X}}_{(r)}(t) + \Big(\alpha_{(r)}A_{2u} - \complement_{(r)}\Big)U_{(r)}(t) + \alpha_{(r)}A_{2w}\Big(W\Big(\overline{\mathcal{X}}_{(r)}(t)\Big) - W\Big(\hat{\overline{\mathcal{X}}}_{(r)}(t)\Big)\Big) \\ + \alpha_{(r)}A_{d1(r)}\bar{D}_{(r),1}(t) + \alpha_{(r)}A_{d2(r)}\bar{D}_{(r),2}(t) - \Big(T_{(r)}\hat{\overline{\mathcal{X}}}_{(r)}(t) - T_{(r)}\theta_{(r)}Y_{(r)}(t) \\ + \lambda_{(r)}y_{(r)}(t) + G_{(r)}\mu_{1(r)}\Big(Y_{(r)}(t) - \hat{Y}_{(r)}(t)\Big) + H_{(r)}R_{1(r)}\mu_{1(r)}\Big(\dot{Y}_{(r)}(t) - \hat{\dot{Y}}_{(r)}(t)\Big)\Big). \end{aligned} \quad (22)$$

Given that $\lambda_{(r)}$ is defined as the sum of $\lambda_{1(r)}$ and $\lambda_{2(r)}$, we can express this as follows:

$$\begin{aligned} \dot{\epsilon}_{(r)}(t) = \alpha_{(r)}A_{2\mathrm{x}}\hat{\overline{\mathcal{X}}}_{(r)}(t) + \epsilon_{(r)}(t)\Big(\alpha_{(r)}A_{2\mathrm{x}} - G_{(r)}\mu_{1(r)}C_{2(r)} - \lambda_{1(r)}C_{2(r)}\Big) \\ + \Big(\alpha_{(\mathrm{k})}A_{2\mathrm{u(k)}} - \complement_{(\mathrm{k})}\Big)U_{(\mathrm{k})}(t) + \alpha_{(r)}A_{2\mathrm{w}}\Big(W\Big(\overline{\mathcal{X}}_{(\mathrm{r})}(t)\Big) - W\Big(\hat{\overline{\mathcal{X}}}_{(\mathrm{r})}(t)\Big)\Big) \\ + \alpha_{(\mathrm{r})}A_{\mathrm{d1(r)}}\bar{D}_{(\mathrm{r}),1}(t) + \alpha_{(\mathrm{r})}A_{\mathrm{d2(r)}}D_{(\mathrm{r}),2}(t) - \Big(T_{(\mathrm{r})}\hat{\overline{\mathcal{X}}}_{(\mathrm{r})}(t) - T_{(\mathrm{r})}\theta_{(\mathrm{r})}Y_{(\mathrm{r})}(t) \\ + \lambda_{1(r)}C_{2(r)}\hat{\overline{\mathcal{X}}}_{(r)}(t) + \lambda_{2(r)}Y_{(r)}(t)\Big) + H_{(r)}R_{1(r)1(r)}C_{2(r)}\Big(\dot{\epsilon}_{(r)}(t)\Big). \end{aligned} \quad (23)$$

By fulfilling the conditions outlined in (24), (27) can be simplified to (25). As a result, it becomes evident that satisfying (24) leads to the decoupling of the variable $\bar{d}_{r,1}(t)$.

$$\begin{aligned} \alpha_{(r)}A_{d1} &= 0, \\ \alpha_{(r)}A_{2\mathrm{u}} &= \complement_{(\mathrm{r})}, \\ \Big(\alpha_{(r)}A_{2\mathrm{x}} - \lambda_{1(r)}C_2\Big)\theta_{(\mathrm{r})} &= \lambda_{2(\mathrm{r})}, \\ \alpha_{(r)}A_{2x} - \lambda_{1(r)}C_2 &= T_{(r)}, \end{aligned} \quad (24)$$

$$\begin{aligned}\dot{\epsilon}_{(r)}(t) &= \left(\alpha_{(r)}A_{2x} - G_{(r)}\mu_{1(r)}C_2 - \lambda_{1(r)}C_2\right)\epsilon_{(r)}(t) + \alpha_{(r)}A_{2\mathrm{w}}\widetilde{W}_{(r)}(t) + \\ &\alpha_{(\mathrm{r})}A_{\mathrm{d2}}\bar{D}_{(\mathrm{r}),2}(t) + H_{(r)}R_{1(r)}\mu_{1(r)}C_2\left(\dot{\epsilon}_{(r)}(t)\right)\left(I - H_{(r)}R_{1(r)}\mu_{1(r)}C_2\right)\dot{\epsilon}_{(r)}(t) \\ &= \left(\alpha_{(r)}A_{2x} - G_{(r)}\mu_{1(r)}C_2 - \lambda_{1(r)}C_2\right)\epsilon_{(r)}(t) + \alpha_{(r)}A_{2\mathrm{w}}\widetilde{W}_{(r)}(t) + \alpha_{(\mathrm{r})}A_{\mathrm{d2}}\bar{D}_{(\mathrm{r}),2}(t),\end{aligned} \tag{25}$$

where $\widetilde{W}_{(r)}(t) = \left(W\left(x_{(r)}(t)\right) - W\left(\widehat{\tilde{x}}_{(r)}(t)\right)\right)$. Equation (25) serves to illustrate that $\bar{d}_{r,1}(t)$ is indeed decoupled under the mentioned conditions.

In the scenario where U is defined as $\left(I - H_{(r)}R_{1(r)}\mu_{1(r)}C_2\right)$,

$$(U)\dot{\epsilon}_{(r)}(t) = \left(\alpha_{(r)}A_{2x} - G_{(r)}\mu_{1(r)}C_2 - \lambda_{1(r)}C_2\right)\epsilon_{(r)}(t) + \alpha_{(r)}A_{2w}\widetilde{W}_{(r)}(t) + \alpha_{(r)}A_{d2}\bar{D}_{(r),2}(t). \tag{26}$$

By performing division by U,

$$\dot{\epsilon}_{(r)}(\mathrm{t}) = \mathrm{U}^{-1}\left(\left(\alpha_{(\mathrm{r})}\mathrm{A}_{2\mathrm{x}(r)} - G_{(\mathrm{r})}\mu_{1(r)}\mathrm{C}_{2(\mathrm{r})} - \lambda_{1(\mathrm{r})}\mathrm{C}_2\right)\epsilon_{(r)}(t) + \alpha_{(\mathrm{r})}\mathrm{A}_{2\mathrm{w}}\widetilde{W}_{(\mathrm{r})}(\mathrm{t}) + \alpha_{(\mathrm{r})}\mathrm{A}_{\mathrm{d2}}\bar{\mathrm{D}}_{(\mathrm{r}),2}(\mathrm{t})\right). \tag{27}$$

When dealing with the error dynamics outlined above, the initial step involves determining APs. A set of guidelines governs the procedure for selecting the APs. Initially, priority is given to constructing the matrix $H_{(r)}$ with rows of full rank, a strategic move aimed at elevating the H_∞ performance in Theorem 1 and consequently decreasing its parameter γ. Subsequent to this, the refinement of γ reduction is pursued by systematically exploring different values for $R_{1(r)}$, utilizing an iterative approach to find the optimal fit. Consequently, the structure of matrix $U = \left(I - H_{(r)}R_{1(r)}\mu_{1(r)}C_2\right)$ is established as a preliminary step preceding the computation of observer gains.

Theorem 1. *Given constants r and O, representing the center and radius of a circular region labeled as $\mathcal{D}(O, r)$, and an adjustable performance threshold for H_∞ denoted as γ, we proceed. Let us assume that the eigenvalues of the matrix $\left(\left(I - \varphi_{(r)}C_2 - G_{1(r)}S_{(r)}C_2\right)A_{2x} - G_{2(r)(r)} - G_{3(r)}C_2\right)$ are situated within the confines of the LMI region $\mathcal{D}(O, r)$. Further, let us assume that the error system (27) demonstrates asymptotic stability. To fulfill these conditions, the following criteria must be met:*

(i) Matrix $\mathcal{P}_r$ is symmetric and positive definite; (ii) the existence of matrices $G_{1(r)}$, $G_{2(r)}$, and $G_{3(r)}$; (iii) a predetermined matrix U; and (iv) the presence of positive real constants L and ρ, which all satisfy the subsequent set of LMIs:

$$\overline{\overline{\prod}} = \begin{bmatrix} \overline{\overline{\prod}}_{11} & \overline{\overline{\prod}}_{12} & \overline{\overline{\prod}}_{13} \\ * & -\gamma I & 0 \\ * & * & -\rho I \end{bmatrix} < 0, \tag{28}$$

$$\begin{bmatrix} -\mathcal{P}_r & \overline{\overline{\prod}}_1 - O(\mathcal{P}_r)U \\ * & -r^2U^T(\mathcal{P}_r)U \end{bmatrix} < 0, \tag{29}$$

where

$$\theta_{(r)} = A_{1d(r)}\left(C_{2(r)}A_{1d(r)}\right)^+ + J_{(r)}\left[I - C_{2(r)}A_{1d(r)} \times \left(C_{2(r)}A_{1d(r)}\right)^+\right] = \varphi_{(r)} + J_{(r)}S_{(r)}, \tag{30}$$

$$\begin{aligned}\left(C_{2(r)}A_{1d(r)}\right)^+ &= \left(\left(C_{2(r)}A_{1d(r)}\right)^T\left(C_{2(r)}A_{1d(r)}\right)\right)^{-1} \times \left(C_{2(r)}A_{1d(r)}\right)^T, \\ \varphi_{(r)} &= A_{1d(r)}\left(C_{2(r)}A_{1d(r)}\right)^+, \\ S_{(r)} &= I - C_{2(r)}A_{1d(r)}\left(C_{2(r)}A_{1d(r)}\right)^+,\end{aligned} \tag{31}$$

and

$$\begin{aligned}\overline{\overline{\Pi}}_1 &= \left(\mathcal{P}_r I - \mathcal{P}_r \varphi_{(r)} C_2 - G_{1(r)} S_{(r)} C_2\right) A_{2x} - G_{2(\mathrm{r})} \mu_{(\mathrm{r})} - G_{3(\mathrm{r})} C_2,\\ \bar{\Pi}_{11} &= (U^T(\mathcal{P}_r I - \mathcal{P}_r \varphi_{(r)} C_2 - G_{1(\mathrm{r})} S_{(\mathrm{r})} C_2) A_{2\mathrm{x}} - G_{2(r)} \mu_{(r)} - G_{3(\mathrm{r})} C_2)^T + ((\mathcal{P}_r I - \mathcal{P}_r \varphi_{(\mathrm{r})} C_2 - G_{1(r)} S_{(r)} C_2) A_{2\mathrm{x}} - \\ &\quad G_{2(\mathrm{r})} \mu_{(\mathrm{r})} - G_{3(r)} C_2 + \rho L^2 I + I) U),\\ \bar{\Pi}_{12} &= U^T \left(\mathcal{P}_r I - \mathcal{P}_r \varphi_{(r)} C_2 - G_{1(\mathrm{r})} S_{(r)} C_2\right) \alpha_{(\mathrm{r})},\\ \bar{\Pi}_{13} &= U^T \left(\mathcal{P}_r I - \mathcal{P}_r \varphi_{(r)} C_2 - G_{1(r)} S_{(r)} C_2\right) A_{2w.}\end{aligned} \tag{32}$$

Moreover, $J_{(r)} = \mathcal{P}_r{}^{-1} G_{1(r)}, G_{(r)} = \mathcal{P}_r{}^{-1} G_{2(r)}$, *and* $\lambda_{1(r)} = \mathcal{P}_r{}^{-1} G_{3(r)}$. *To enhance estimation performance, LMIs are solved using the Yet Another Linear Matrix Inequality Parser (YALMIP) optimization toolbox in MATLAB, where the adjustable parameter* γ *in LMIs is optimized to minimize* H_∞ *performance. Furthermore, to optimize execution time, the YALMIP framework has been enhanced by integrating the Toh–Todd–Tütüncü (SDPT3) solver from semidefinite programming. Therefore, simulations are conducted in MATLAB, utilizing YALMIP for solving LMIs and integrating SDPT3 to efficiently manage inequalities within the semidefinite programming framework.*

Proof. The Lyapunov function for rth agent is defined as follows [13]:

$$V_r = \epsilon_{(r)}^T \left(U^T \mathcal{P}_r U\right) \epsilon_{(r)}, \mathcal{P}_r > 0. \tag{33}$$

Using (27), we have

$$\begin{aligned}\dot{V}_r = \dot{\epsilon}_{(r)}^T (U^T \mathcal{P}_r U) \epsilon_{(r)} + \epsilon_{(r)}^T (U^T \mathcal{P}_r U) \dot{\epsilon}_{(r)} = \left(\mathrm{U}^{-1}\left(\left(\alpha_{(\mathrm{r})} \mathrm{A}_{2\mathrm{x}(r)} - G_{(\mathrm{r})} \mu_{1(r)} C_{2(\mathrm{r})} - \lambda_{1(\mathrm{r})} C_2\right) \epsilon_{(r)}(\mathrm{t})\right.\right.\\ \left.\left. + \alpha_{(\mathrm{r})} \mathrm{A}_{2\mathrm{w}} \widetilde{W}_{(\mathrm{r})}(\mathrm{t}) + \alpha_{(\mathrm{r})} \mathrm{A}_{\mathrm{d2}} \bar{\mathrm{D}}_{(\mathrm{r}),2}(\mathrm{t})\right)^T (U^T \mathcal{P}_r U) \epsilon_{(r)} + \epsilon_{(r)}^T (U^T \mathcal{P}_r U)\\ \left(\mathrm{U}^{-1}\left(\left(\alpha_{(\mathrm{r})} \mathrm{A}_{2\mathrm{x}(r)} - G_{(\mathrm{r})} \mu_{1(r)} C_{2(\mathrm{r})} - \lambda_{1(\mathrm{r})} C_2\right) \epsilon_{(r)}(\mathrm{t}) + \alpha_{(\mathrm{r})} \mathrm{A}_{2\mathrm{w}} \widetilde{W}_{(\mathrm{r})}(\mathrm{t}) + \alpha_{(\mathrm{r})} \mathrm{A}_{\mathrm{d2}} \bar{\mathrm{D}}_{(\mathrm{r}),2}(\mathrm{t})\right)^T.\end{aligned} \tag{34}$$

Further simplifying the above equation gives the following:

$$\begin{aligned}\dot{V}_r = \epsilon_{(r)}^T \left(\left(\mathrm{U}^{-1}\left(\left(\alpha_{(\mathrm{r})} \mathrm{A}_{2\mathrm{x}(r)} - G_{(\mathrm{r})} \mu_{1(r)} C_{2(\mathrm{r})} - \lambda_{1(\mathrm{r})} C_2\right)^T (U^T \mathcal{P}_r U)\right.\right.\\ + (U^T \mathcal{P}_r U)\left(\mathrm{U}^{-1}\left(\left(\alpha_{(\mathrm{r})} \mathrm{A}_{2\mathrm{x}(r)} - G_{(\mathrm{r})} \mu_{1(r)} C_{2(\mathrm{r})} - \lambda_{1(\mathrm{r})} C_2\right)\right)\epsilon_{(r)}\\ \left. + 2\mathrm{U}^{-1}\left(\epsilon_{(r)}^T(t)(U^T \mathcal{P}_r U) \alpha_{(\mathrm{r})} \mathrm{A}_{2\mathrm{w}} \widetilde{W}_{(\mathrm{r})}(\mathrm{t})\right) + 2\mathrm{U}^{-1}\left(\epsilon_{(r)}^T(t)(U^T \mathcal{P}_r U) \alpha_{(\mathrm{r})} \mathrm{A}_{\mathrm{d2}} \bar{\mathrm{D}}_{(\mathrm{r}),2}(\mathrm{t})\right).\end{aligned} \tag{35}$$

Considering $\mathrm{p}_{(\mathrm{r})} = \left(\alpha_{(\mathrm{r})} \mathrm{A}_{2\mathrm{x}(\mathrm{r})} - G_{(\mathrm{r})} \mu_{1(\mathrm{r})} C_{2(\mathrm{r})} - \lambda_{1(\mathrm{r})} C_2\right)$, (34) can be defined as

$$\begin{aligned}\dot{V}_r(t) = \epsilon_{(r)}^T(t) \mathrm{U}^{-1}\left(\left(p_{(r)}\right)^T (U^T \mathcal{P}_r U) + (U^T \mathcal{P}_r U) p_{(r)}\right)\epsilon_{(r)}\\ + 2U^{-1}\left(\epsilon_{(r)}^T(t)(U^T \mathcal{P}_r U) \alpha_{(\mathrm{r})} A_{2w} \widetilde{W}_{(r)}(t)\right) + 2U^{-1}\left(\epsilon_{(r)}^T(t)(U^T \mathcal{P}_r U) \alpha_{(\mathrm{r})} A_{d2} \bar{D}_{(r),2}(t)\right).\end{aligned} \tag{36}$$

From Lemma 2,

$$2\epsilon_{(r)}\left(U^T \mathcal{P}_r U\right) \alpha_{(\mathrm{r})} \mathrm{A}_{2\mathrm{w}} \widetilde{W}_{(r)} \leq \left(\frac{1}{\rho}\right) \epsilon_{(r)}^T(t)\left(U^T \mathcal{P}_r U\right) \alpha_{(\mathrm{r})} \times \mathrm{A}_{2\mathrm{w}}\left(\left(U^T \mathcal{P}_r U\right) \alpha_{(\mathrm{r})} \mathrm{A}_{2\mathrm{w}}\right)^T \epsilon_{(r)}(t) + \rho \widetilde{W}_{(\mathrm{r})}^T \widetilde{W}_{(\mathrm{r})}. \tag{37}$$

From (3), for a one-sided Lipschitz non-linear function, we have

$$\begin{aligned}\widetilde{W}_{(r)}^T \widetilde{W}_{(r)} = \left(\widetilde{W}_r^r\right)^T \left(\widetilde{W}_r^r\right) + \left(\widetilde{W}_r^j\right)^T \left(\widetilde{W}_r^j\right) + \cdots + \left(\widetilde{W}_r^N\right)^T \left(\widetilde{W}_r^N\right) \leq L^2 \| \overline{\mathcal{X}}_r^r - \hat{\overline{\mathcal{X}}}_r^r \|^2 + \cdots\\ + L_{|N|}^2 \| \overline{\mathcal{X}}_r^N - \hat{\overline{\mathcal{X}}}_r^N \|^2 \leq L^2 \left(\| \overline{\mathcal{X}}_{r1} - \hat{\overline{\mathcal{X}}}_{r1} \|^2 + \cdots + \| \overline{\mathcal{X}}_r^N - \hat{\overline{\mathcal{X}}}_r^N \|^2\right) \leq L^2 \epsilon_{(\mathrm{r})}^T \epsilon_{(\mathrm{r})},\end{aligned} \tag{38}$$

where $\widetilde{W}_{(r)} = \left(W\left(\overline{\mathcal{X}}_{(r)}(t)\right) - W\left(\hat{\overline{\mathcal{X}}}_{(r)}(t)\right)\right)$ and $L = max\{L_{rk}\}, k \in \{1, \ldots, \mathrm{R}\}$. For a constant ρ:

$$\rho L^2 \epsilon_{(r)}^T \epsilon_{(r)} - \rho \widetilde{W}_{(r)}^T \widetilde{W}_{(\mathrm{r})}(t) \geq 0. \tag{39}$$

Assume $\bar{D}_{(r),2}(t) = 0$. Using (37), we can rewrite (39) as

$$\dot{V}_r = \epsilon_{(r)}^T \mathrm{U}^{-1}\Big(\Big(p_{(r)}\Big)^T (U^T\mathcal{P}_r U) + (U^T\mathcal{P}_r U)p_{(r)} + (1/\rho)(U^T\mathcal{P}_r U)\alpha_{(\mathrm{r})}\mathrm{A}_{2\mathrm{w}}, \times\Big((U^T\mathcal{P}_r U)\alpha_{(r)}A_{2w}\Big)^T + \rho L^2 I\Big)\epsilon_{(r)}(t)\Big) < 0. \tag{40}$$

Using the Schur decomposition, the next inequality can be defined:

$$v_r = \begin{bmatrix} \prod_{11} & \mathcal{P}_r\alpha_{(r)}A_{2w} \\ * & -\rho I \end{bmatrix} < 0, \tag{41}$$

where

$$\prod_{11} = U^{-1}\Big(p_{(r)}\Big)^T\Big(U^T\mathcal{P}_r U\Big) + \Big(U^T\mathcal{P}_r U\Big)p_{(r)} + \rho L^2. \tag{42}$$

If the non-equality (40) is satisfied, then $\dot{V}_r < 0$ and the error dynamics are stable. Examining the case where $\bar{D}_{(r),2}(t) \neq 0$. One can define $\prod_r$ as

$$\prod_r = \int_0^{T_f} \Big(\epsilon_{(r)}^T\epsilon_{(r)} - \gamma\bar{D}_{(r),2}(t)^T\bar{D}_{(r),2}(t)\Big)dt. \tag{43}$$

From (34),

$$\prod_r = \int_0^{T_f} \Big(\epsilon_{(r)}^T\epsilon_{(r)} - \gamma\bar{D}_{(r),2}(t)^T\bar{D}_{(r),2}(t) + \dot{V}_r\Big)dt - \int_0^{T_f} \dot{V}_r dt. \tag{44}$$

Using the new $\prod_r$, (43) can be rewritten as

$$\begin{matrix} \prod_r = \int_0^{T_f} \begin{bmatrix} \epsilon_{(r)}^T & \bar{D}_{(r),2}(t)^T \end{bmatrix}, \\ \Pi\begin{bmatrix} \epsilon_{(r)} \\ \bar{D}_{(r),2}(t) \end{bmatrix}dt - \int_0^{T_f} \dot{V}_r dt, \end{matrix} \tag{45}$$

where

$$\Pi = \begin{bmatrix} \Pi_{11} & U^T\mathcal{P}_r\alpha_{(r)}A_{d2}\bar{D}_{(r),2}(t) \\ * & -\gamma I \end{bmatrix} \tag{46}$$

and

$$\Pi_{11} = \Gamma_{11} + \left(\frac{1}{\rho}\right)U^T\mathcal{P}_r\alpha_{(\mathrm{r})}\mathrm{A}_{2\mathrm{w}}\Big(\mathcal{P}_r\alpha_{(\mathrm{r})}\mathrm{A}_{2\mathrm{w}}\Big)^T + \mathrm{I}. \tag{47}$$

Using Schur decomposition, the Π is equivalent to

$$\overline{\Pi} = \begin{bmatrix} U^T\Big(\Big(p_{(r)}\Big)^T\mathcal{P}_r + \mathcal{P}_r p_{(r)} + \rho L^2\mathrm{I} + \mathrm{I}\Big) & \mathcal{P}_r\alpha_{(r)}A_{d2} & \mathcal{P}_r\alpha_{(\mathrm{r})}\mathrm{A}_{2\mathrm{w}} \\ * & -\gamma\mathrm{I} & 0 \\ * & * & -\rho\mathrm{I} \end{bmatrix}. \tag{48}$$

Recalling $\alpha_{(r)} = I - \beta_{(r)}C_{2(r)}$ and using (30) yields

$$\alpha_{(r)} = \Big(\mathrm{I} - \varphi_{(r)}\mathrm{C}_{2(\mathrm{r})} - J_{(\mathrm{r})}\mathrm{S}_{(\mathrm{r})}\mathrm{C}_{2(\mathrm{r})}\Big). \tag{49}$$

Substituting inequality $\alpha_{(r)}$ into $\overline{\Pi}$, gives

$$\overline{\prod} = \begin{bmatrix} \overline{\Pi}_{11} & \overline{\Pi}_{12} & \overline{\Pi}_{13} \\ * & -\gamma I & 0 \\ * & * & -\rho I \end{bmatrix}, \tag{50}$$

where

$$\begin{aligned}\bar{\Pi}_{11} = \Big(U^T\Big(\mathcal{P}_r I - \mathcal{P}_r\varphi_{(r)}C_2 - G_{1(\mathrm{r})}S_{(\mathrm{r})}C_2\Big)A_{2\mathrm{x}} - G_{2(r)(r)} - G_{3(\mathrm{r})}C_2\Big)^T + \Big(\Big(\mathcal{P}_r I - \mathcal{P}_r\varphi_{(\mathrm{r})}C_2 \\ - G_{1(r)}S_{(r)}C_2\Big)A_{2\mathrm{x}} - G_{2(\mathrm{r})(\mathrm{r})} - G_{3(r)}C_2 + \rho L^2 I + I\Big)U), \\ \bar{\Pi}_{12} = U^T\Big(\mathcal{P}_r I - \mathcal{P}_r\varphi_{(r)}C_2 - G_{1(\mathrm{r})}S_{(r)}C_2\Big)\alpha_{(\mathrm{r})}, \\ \bar{\Pi}_{13} = U^T\Big(\mathcal{P}_r I - \mathcal{P}_r\varphi_{(r)}C_2 - G_{1(r)}S_{(r)}C_2\Big)A_{2w}.\end{aligned} \tag{51}$$

By substituting $G_{1(r)} = \mathcal{P}_r J_{(r)}$, $G_{2(r)} = \mathcal{P}_r G_{(r)}$, and $G_{3(r)} = \mathcal{P}_r\lambda_{1(r)}$ into (49), using Lemma 1 reveals that the eigenvalues of $\Big(\Big(I - \varphi_{(r)}C_2 - G_{1(r)}S_{(r)}C_2\Big)A_{2x} - G_{2(r)}\mu_{(r)} - G_{3(r)}C_2\Big)$ reside in $D(O,r)$, which means proof of Theorem 1 is complete. □

3. Results and Discussion

This section provides simulation results for fault detection and estimation methods discussed earlier. The simulations were run on a Windows computer Dell Precision T1700 series with one Intel Xenon Quad Core central processing unit (CPU) of 3.50 GHz power, 16 GB of random access memory (RAM), and a Nvidia Quadro K620 graphics card with 2 GB memory. Figure 1 depicts an assembly of five small communication satellites under a directed communication topology, with two identified as faulty (highlighted in red). The configuration consists of two clusters, where satellites within each cluster share a common goal different from those in the other cluster.

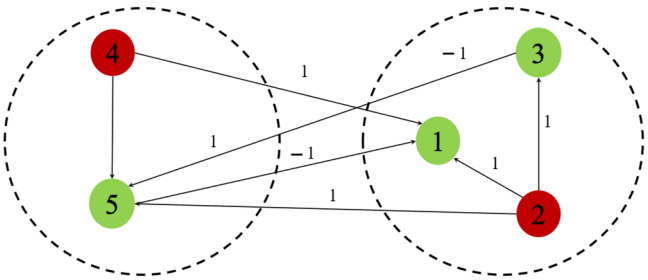


Figure 1. Communication topology.

A mathematical representation of a geostationary communications satellite positioned in the Earth's equatorial plane was developed in [44]. This involved creating a linearized state–space model tailored explicitly for the satellite's geostationary orbit. The state–space model of the current research incorporates non-linearity by introducing a one-sided Lipschitz non-linear function. Considering (1) and (2), the depiction of the one-sided Lipschitz non-linear satellite model is presented in (52). Where there are four states, namely, $x_1 = R = \frac{r}{R_e} = \frac{R_e + h_0}{R_e}$, $x_2 = \theta$, $x_3 = \dot{R}$, $x_4 = \dot{\theta}$ [44], and R_e is the Earth's radius, h_0 is the altitude of the communication satellite measured from the Earth's surface, and θ indicates the circular movement of the satellite with respect to the reference axis.

$$A_{1x} = \begin{bmatrix} 0 & 1 & 0 & 0 \\ 0 & 0 & 0 & 1 \\ 0.01036 & -0.01 & 0 & 0.7753 \\ 0 & 0 & -0.1774 & 0 \end{bmatrix},$$
$$A_{1u} = \begin{bmatrix} 0 & 0 \\ 0 & 0 \\ 1 & 0 \\ 0 & 0.1511 \end{bmatrix}, A_{1f} = \begin{bmatrix} 1 \\ 1 \\ 1 \\ 1 \end{bmatrix}, A_{1w} = \begin{bmatrix} 0.2 \\ 0 \\ 0 \\ 0 \end{bmatrix}, \quad (52)$$
$$A_{1d} = \begin{bmatrix} -0.01 & 0.02 \\ -0.2 & 0.01 \\ 0.2 & -0.02 \\ 0.01 & 0.2 \end{bmatrix}, C_1 = \begin{bmatrix} 1 & 0 & 0 & 0 \\ 0 & 1 & 0 & 0 \\ 0 & 0 & 1 & 0 \end{bmatrix}$$

Since the number of outputs is less than the unknown inputs, the disturbances can be decoupled partially [12]. This means, as explained in Assumption 1, that $d_{r,1}(t)$ can undergo decoupling. We account for the satellites' one-sided Lipschitz non-linear parts using the following:

$$w_{1-7}(x_{1-7}(t)) = (x_{1-7}(t))^2 sin(x_{1-7}(t)). \quad (53)$$

The disturbance vectors for satellites within distinct clusters differ from those of satellites in other clusters due to variations in the operational and environmental conditions. The external disturbances in the first and second clusters are illustrated below:

$$\begin{aligned} d_{1-3}(t) &= [5cos(t)5cos(t)]^T, \\ d_{4-5}(t) &= [2sin(4t)2sin(4t)]^T. \end{aligned} \quad (54)$$

This study focuses on component faults, specifically sudden actuator faults along all four axis states. We have two faulty satellites with the simultaneous faults outlined as follows:

$$f_2(t) = \begin{cases} 100sin(30t) + 70cos(t) & 2\text{s} \leq t < 6\text{s} \\ t - 100 & 7\text{s} \leq t < 14\text{s} \\ t & 16\text{s} \leq t < 18\text{s} \\ 0 & other \end{cases},$$
$$f_4(t) = \begin{cases} 20cos(t) & 4\text{s} \leq t < 10\text{s} \\ 12cos(100t) + 18cos(10t) & 11\text{s} \leq t < 15\text{s} \\ 0 & other. \end{cases} \quad (55)$$

Leveraging the insights in this paper, the fault and state estimator embedded within satellite 1 demonstrates the capacity to approximate the faults transpiring in satellites 2 and 4, which are susceptible to faults.

In the following figures, the term A# denotes agent number # or satellite number #. This abbreviation is used for brevity. To identify the fault, residuals are computed using (19). Figure 2 illustrates that the observer incorporated within satellite 1 can detect the faults occurring in satellites 2 and 4, which are part of a distinct cluster. By analyzing Figure 2, it is possible to detect the occurrence time for faults and their corresponding satellites to isolate them at a suitable time.

The outcomes of the fault estimation simulation are depicted in Figures 3 and 4. As can be seen in Figure 3, the observer integrated within satellite 1 can estimate the faults occurring in satellites 2 and 4, which belong to a different cluster.

As shown in Figure 5, the fault estimation for the UIO established on satellite 2 is compared with the AP-based one. The results in Table 1 emphasize that the H_∞ performance level will improve by selecting appropriate APs. Furthermore, as shown in Table 2, significant improvements in fault estimation root mean square error (RMSE) have been achieved, with an average reduction of approximately 56.61% in the difference between actual and estimated fault values using two approaches: robust UIO and AP-based robust UIO.

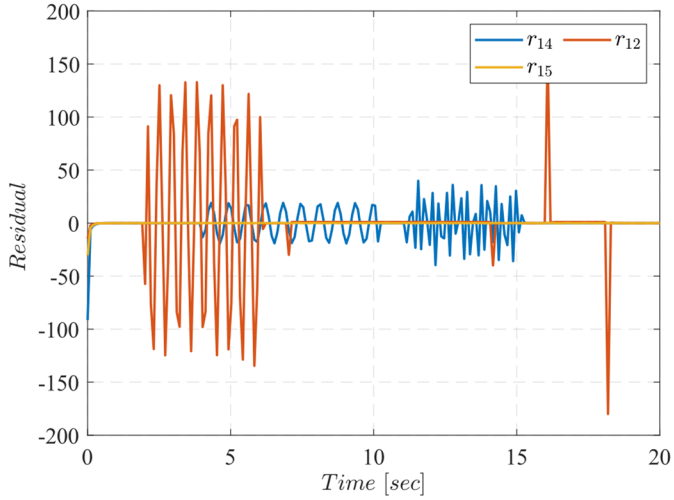


Figure 2. State residual generated by A1.

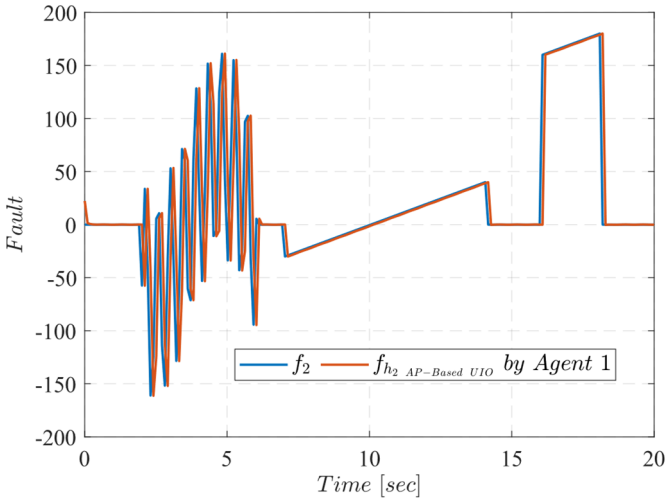


Figure 3. Fault in A2 estimated by AP-based UIO on A1.

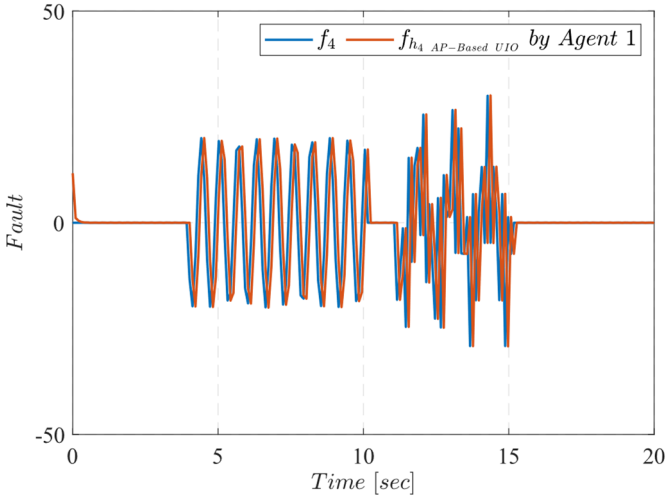


Figure 4. Fault in A4 estimated by AP-based UIO on A1.

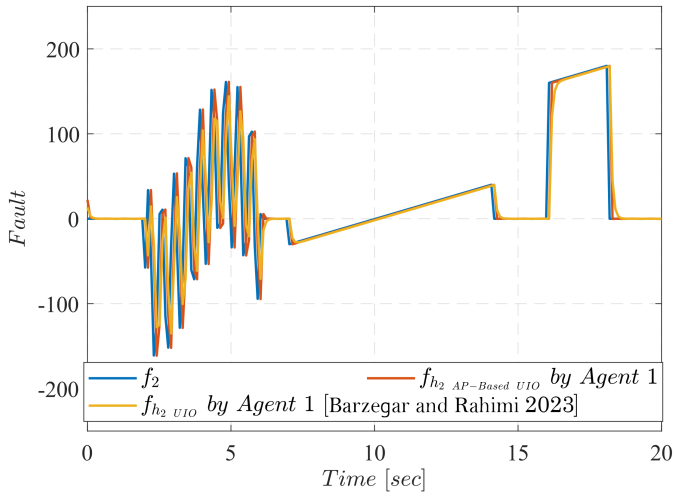


Figure 5. Fault estimation by AP-based and simple UIO [25].

Table 1. Robust observer performance level comparison.

Observation Type	Performance Level
General Robust UIO	$\gamma = 1.12$
AP-Based Robust UIO	$\gamma = 0.85$

Table 2. Fault estimation error comparison.

Max RMSE	Fault-Free	During Fault
Robust UIO	0.0436	1.252
AP-Based Robust UIO	0.0211	0.5432

A circular region with a center at -7 and a radius of 1.5 is used to avoid excessively high observer gains. From (29), this restriction is implemented through the LMI.

After numerous trials, we determined that $H_{(r)}=\begin{bmatrix}1 & 0\\ 0 & 1\end{bmatrix}$ and $R_{1(r)}$ =2.8 are the best-suited APs. It is essential to mention that similar to other constant matrices in (10), matrix $H_{(r)}$ should undergo dimension expansion using the Kronecker product. This expansion plays a vital role in ensuring that the dimensions are appropriately aligned for global observer design (14), where the dimension of constant matrices in each satellite depends on the number of its neighbors.

4. Future Research Directions

Future research directions could include developing algorithms for groups of agents with different dynamics addressing the heterogeneity in MASs. This heterogeneity could involve having different system orders. Additionally, exploring various forms of topology, such as switching topology, could effectively isolate faulty agents.

Furthermore, as the current study focuses on model-based fault diagnosis, integrating a hybrid approach that combines model-based and data-driven methods could potentially overcome each method's inherent limitations. This integration could pave the way for more advanced analytical techniques in fault diagnosis.

Finally, future research could evaluate the system's performance under different nonlinearities and investigate its quadratically inner-bounded properties. Additionally, the application of the AP-based method to other observers can be explored.

5. Conclusions

This study presents a fault diagnosis method using APs for MASs. Simulation results demonstrated that adding APs to robust UIO can enhance precision and design flexibility.

We also developed a distributed time-varying failure estimation and detection system for satellite clusters. Our approach, integrating UIO, minimizes external disturbance effects, ensuring robustness. The case study involving one-sided Lipschitz non-linear satellite clusters operating in diverse environments showcased the effectiveness of our approach in detecting multiple simultaneous time-varying faults. The result is compared with the fault diagnosis approach using general UIO in [25] to highlight the potential of the AP-based UIO fault diagnosis method. Although the methods in this study were tested on a singular implementation, they can be applied to any multi-agent system topology, accommodating various numbers of healthy and faulty agents with different forms of communication, including directed and undirected graphs.

Author Contributions: Conceptualization, A.B. and A.R.; methodology, A.B.; software, A.B. and A.R.; validation, A.B.; formal analysis, A.B.; investigation, A.B.; resources, A.R.; data curation, A.B.; writing—original draft preparation, A.B.; writing—review and editing, A.R.; visualization, A.B. and A.R.; supervision, A.R.; project administration, A.R.; funding acquisition, A.R. All authors have read and agreed to the published version of the manuscript.

Funding: This research was funded by the Natural Sciences and Engineering Research Council of Canada (NSERC) Discovery grant number RGPIN-2020-05513, and the APC was funded by RGPIN-2020-05513.

Data Availability Statement: The original contributions presented in the study are included in the article, further inquiries can be directed to the corresponding author/s.

Acknowledgments: The authors would like to thank the Natural Sciences and Engineering Research Council of Canada and the University of Windsor, Canada, for their financial and strategic support during this work.

Conflicts of Interest: The authors declare no conflicts of interest.

References

1. Li, Z.; Zhisheng, D. *Cooperative Control of Multi-Agent Systems*; CRC Press: Boca Raton, FL, USA, 2017. [CrossRef]
2. Barzegar, A.; Rahimi, A. Fault Diagnosis and Prognosis for Satellite Formation Flying: A Survey. *IEEE Access* **2022**, *10*, 26426–26442. [CrossRef]
3. Amirkhani, A.; Barshooi, A.H. Consensus in multi-agent systems: A review. *Artif. Intell. Rev.* **2021**, *55*, 3897–3935. [CrossRef]
4. Zhang, D.; Feng, G.; Shi, Y.; Srinivasan, D. Physical Safety and Cyber Security Analysis of Multi-Agent Systems: A Survey of Recent Advances. *IEEE/CAA J. Autom. Sin.* **2021**, *8*, 319–333. [CrossRef]
5. Phadke, A.; Medrano, F.A. Towards Resilient UAV Swarms—A Breakdown of Resiliency Requirements in UAV Swarms. *Drones* **2022**, *6*, 340. [CrossRef]
6. Roche, R.; Blunier, B.; Miraoui, A.; Hilaire, V.; Koukam, A. Multi-agent systems for grid energy management: A short review. In Proceedings of the IECON 2010—36th Annual Conference on IEEE Industrial Electronics Society, Glendale, AZ, USA, 7–10 November 2010; IEEE: Piscataway, NJ, USA, 2010. [CrossRef]
7. Chen, M.-Y.; Chen, C.-T.; Huang, S.-H. Knowledge distillation for portfolio management using multi-agent reinforcement learning. *Adv. Eng. Inform.* **2023**, *57*, 102096. [CrossRef]
8. Rahimi, A.; Kumar, K.D.; Alighanbari, H. Fault detection and isolation of control moment gyros for satellite attitude control subsystem. *Mech. Syst. Signal Process.* **2020**, *135*, 106419. [CrossRef]
9. Rahimi, A.; Kumar, K.D.; Alighanbari, H. Fault estimation of satellite reaction wheels using covariance based adaptive unscented Kalman filter. *Acta Astronaut.* **2017**, *134*, 159–169. [CrossRef]
10. Farahani, H.V.; Rahimi, A. Data-Driven Fault Diagnosis for Satellite Control Moment Gyro Assembly with Multiple In-Phase Faults. *Electronics* **2021**, *10*, 1537. [CrossRef]
11. Zhang, K.; Jiang, B.; Shi, P.; Cocquempot, V. *Observer-Based Fault Estimation Techniques*; Springer International Publishing: Berlin/Heidelberg, Germany, 2018. [CrossRef]
12. Barzegar, A.; Rahimi, A. A dissipativity-based robust fault diagnosis approach for clusters of small satellites. *Acta Astronaut.* **2024**, *214*, 182–195. [CrossRef]
13. Barzegar, A.; Rahimi, A. Distributed Simultaneous Fault Estimation and Cluster Consensus Control of Small Satellites. *IEEE Trans. Aerosp. Electron. Syst.* **2023**, *59*, 7654–7665. [CrossRef]
14. Wang, X.; Yang, G.-H. Fault-tolerant consensus tracking control for linear multiagent systems under switching directed network. *IEEE Trans. Cybern.* **2020**, *50*, 1921–1930. [CrossRef] [PubMed]
15. Liu, C.; Jiang, B.; Patton, R.J.; Zhang, K. Decentralized output sliding-mode fault-tolerant control for heterogeneous multiagent systems. *IEEE Trans. Cybern.* **2020**, *50*, 4934–4945. [CrossRef] [PubMed]

16. Yang, H.; Han, Q.-L.; Ge, X.; Ding, L.; Xu, Y.; Jiang, B.; Zhou, D. Fault-Tolerant Cooperative Control of Multi-agent Systems: A Survey of Trends and Methodologies. *IEEE Trans. Ind. Inform.* **2020**, *16*, 4–17. [CrossRef]
17. Mousavi, S.; Khorasani, K. Fault detection of reaction wheels in attitude control subsystem of formation flying satellites. *Int. J. Intell. Unmanned Syst.* **2014**, *2*, 2–26. [CrossRef]
18. Nemati, F.; Hamami, S.M.S.; Zemouche, A. A non-linear observer-based approach to fault detection, isolation and estimation for satellite formation flight application. *Automatica* **2019**, *107*, 474–482. [CrossRef]
19. Valdes, A.; Khorasani, K. A pulsed plasma thruster fault detection and isolation strategy for formation flying of satellites. *Appl. Soft Comput.* **2010**, *10*, 746–758. [CrossRef]
20. Azizi, S.; Khorasani, K. A distributed Kalman filter for actuator fault estimation of deep space formation flying satellites. In Proceedings of the 2009 3rd Annual IEEE Systems Conference, Vancouver, BC, Canada, 23–26 March 2009; IEEE: Piscataway, NJ, USA, 2009. [CrossRef]
21. Azizi, S.M.; Khorasani, K. A hybrid and switching framework for cooperative actuator fault estimation of formation flying satellites in deep space. In Proceedings of the 2009 7th Asian Control Conference, Hong Kong, China, 27–29 August 2009; pp. 1126–1131.
22. Ghasemi, S.; Khorasani, K. Fault detection and isolation of the attitude control subsystem of spacecraft formation flying using extended Kalman filters. *Int. J. Control* **2015**, *88*, 2154–2179. [CrossRef]
23. Meskin, N.; Khorasani, K. Fault Detection and Isolation of Actuator Faults in Spacecraft Formation Flight. In Proceedings of the 45th IEEE Conference on Decision and Control, San Diego, CA, USA, 13–15 December 2006; pp. 1159–1164. [CrossRef]
24. Han, W.; Wang, Z.; Shen, Y. Robust H∞ fault diagnosis observer design for multiple satellites attitude synchronization with disturbance. In Proceedings of the 2016 35th Chinese Control Conference (CCC), Chengdu, China, 27–29 July 2016; pp. 6575–6580. [CrossRef]
25. Barzegar, A.; Rahimi, A. A Distributed Fault Detection and Estimation for Formation of Clusters of Small Satellites. In Proceedings of the 2023 IEEE International Conference on Prognostics and Health Management (ICPHM), Montreal, QC, Canada, 5–7 June 2023; pp. 1–11. [CrossRef]
26. Gao, M.; Yang, S.; Sheng, L. Distributed Fault Estimation for Time-Varying Multi-Agent Systems With Sensor Faults and Partially Decoupled Disturbances. *IEEE Access* **2019**, *7*, 147905–147913. [CrossRef]
27. Zhang, K.; Jiang, B.; Cocquempot, V. Adaptive technique-based distributed fault estimation observer design for multi-agent systems with directed graphs. *IET Control Theory Appl.* **2015**, *9*, 2619–2625. [CrossRef]
28. Zhang, K.; Jiang, B.; Shi, P. Adjustable Parameter-Based Distributed Fault Estimation Observer Design for Multi-agent Systems With Directed Graphs. *IEEE Trans. Cybern.* **2016**, *47*, 306–314. [CrossRef]
29. Rahimi, F.; Ahmadpour, S. Neighborhood-based distributed robust unknown input observer for fault estimation in non-linear networked systems. *IET Control Theory Amp; Appl.* **2022**, *16*, 972–984. [CrossRef]
30. Zhang, K.; Jiang, B.; Shi, P. Distributed Fault Estimation Observer Design With Adjustable Parameters for a Class of Non-linear Interconnected Systems. *IEEE Trans. Cybern.* **2019**, *49*, 4219–4228. [CrossRef] [PubMed]
31. Yang, R.; Feng, Z. BRB-based distributed fault diagnosis for consensus of heterogeneous multi-agent systems. In Proceedings of the 2021 IEEE 23rd Int Conf on High Performance Computing & Communications; 7th Int Conf on Data Science & Systems; 19th Int Conf on Smart City; 7th Int Conf on Dependability in Sensor, Cloud & Big Data Systems & Application (HPCC/DSS/SmartCity/DependSys), Haikou, China, 20–22 December 2021; pp. 1171–1177. [CrossRef]
32. Chadli, M.; Davoodi, M.; Meskin, N. Distributed state estimation, fault detection and isolation filter design for heterogeneous multi-agent linear parameter-varying systems. *IET Control Theory Appl.* **2017**, *11*, 254–262. [CrossRef]
33. Davoodi, M.R.; Khorasani, K.; Talebi, H.A.; Momeni, H.R. Distributed Fault Detection and Isolation Filter Design for a Network of Heterogeneous Multi-agent Systems. *IEEE Trans. Control Syst. Technol.* **2014**, *22*, 1061–1069. [CrossRef]
34. Guo, X.-G.; Liu, P.-M.; Wang, J.-L.; Ahn, C.K. Event-Triggered Adaptive Fault-Tolerant Pinning Control for Cluster Consensus of Heterogeneous Non-linear Multi-Agent Systems Under Aperiodic DoS Attacks. *IEEE Trans. Netw. Sci. Eng.* **2021**, *8*, 1941–1956. [CrossRef]
35. Cai, X.; Lin, Y.; Hong, S. Stabilisation for one-sided Lipschitz non-linear differential inclusions. *IET Control. Theory Appl.* **2013**, *7*, 2172–2177. [CrossRef]
36. Rehan, M.; Jameel, A.; Ahn, C.K. Distributed Consensus Control of One-Sided Lipschitz Non-linear Multi-agent Systems. *IEEE Trans. Syst. Man Cybern. Syst.* **2018**, *48*, 1297–1308. [CrossRef]
37. Razaq, M.A.; Rehan, M.; Ahn, C.K.; Khan, A.Q.; Tufail, M. Consensus of One-Sided Lipschitz Multi-agents Under Switching Topologies. *IEEE Trans. Syst. Man Cybern. Syst.* **2019**, *51*, 1485–1495. [CrossRef]
38. Agha, R.; Rehan, M.; Ahn, C.K.; Mustafa, G.; Ahmad, S. Adaptive Distributed Consensus Control of One-Sided Lipschitz Non-linear Multi-agents. *IEEE Trans. Syst. Man Cybern. Syst.* **2019**, *49*, 568–578. [CrossRef]
39. Yang, W.; Dong, J. Distributed fault-tolerant consensus for one-sided Lipschitz multi-agent systems based on error decomposition and jointly observable condition. *Inf. Sci.* **2024**, *657*, 119994. [CrossRef]
40. Chen, F.; Lu, D.; Li, X. Robust Observer Based Fault-tolerant Control for One-sided Lipschitz Markovian Jump Systems with General Uncertain Transition Rates. *Int. J. Control Autom. Syst.* **2019**, *17*, 1614–1625. [CrossRef]
41. Chilali, M.; Gahinet, P. H/sub ∞/ design with pole placement constraints: An LMI approach. *IEEE Trans. Autom. Control* **1996**, *41*, 358–367. [CrossRef]

42. Liu, X.; Gao, X.; Han, J. Distributed Fault Estimation for a Class of Non-linear Multi-agent Systems. *IEEE Trans. Syst. Man Cybern. Syst.* **2020**, *50*, 3382–3390. [CrossRef]
43. Luo, X.; Han, N.; Guan, X. Leader-following consensus protocols for formation control of multi-agent network. *J. Syst. Eng. Electron.* **2011**, *22*, 991–997. [CrossRef]
44. Hla, M.; Lae, Y.; Kyaw, S.; Zaw, M. Implementation of a Communication Satellite Orbit Controller Design Using State Space Techniques. *ASEAN J. Sci. Technol. Dev.* **2012**, *29*, 29. [CrossRef]

Disclaimer/Publisher's Note: The statements, opinions and data contained in all publications are solely those of the individual author(s) and contributor(s) and not of MDPI and/or the editor(s). MDPI and/or the editor(s) disclaim responsibility for any injury to people or property resulting from any ideas, methods, instructions or products referred to in the content.